AGU100 ADVANCING EARTH AND SPACE SCIENCE

Geophysical Research Letters

RESEARCH LETTER
10.1029/2019GL085782

Causes of Higher Climate Sensitivity in CMIP6 Models

Mark D. Zelinka[1], Timothy A. Myers[1], Daniel T. McCoy[2], Stephen Po-Chedley[1], Peter M. Caldwell[1], Paulo Ceppi[3], Stephen A. Klein[1], and Karl E. Taylor[1]

[1]Lawrence Livermore National Laboratory, Livermore, CA, USA, [2]Institute of Climate and Atmospheric Sciences, University of Leeds, Leeds, UK, [3]Grantham Institute, Imperial College London, London, UK

Abstract Equilibrium climate sensitivity, the global surface temperature response to CO_2 doubling, has been persistently uncertain. Recent consensus places it likely within 1.5–4.5 K. Global climate models (GCMs), which attempt to represent all relevant physical processes, provide the most direct means of estimating climate sensitivity via CO_2 quadrupling experiments. Here we show that the closely related effective climate sensitivity has increased substantially in Coupled Model Intercomparison Project phase 6 (CMIP6), with values spanning 1.8–5.6 K across 27 GCMs and exceeding 4.5 K in 10 of them. This (statistically insignificant) increase is primarily due to stronger positive cloud feedbacks from decreasing extratropical low cloud coverage and albedo. Both of these are tied to the physical representation of clouds which in CMIP6 models lead to weaker responses of extratropical low cloud cover and water content to unforced variations in surface temperature. Establishing the plausibility of these higher sensitivity models is imperative given their implied societal ramifications.

Plain Language Summary The severity of climate change is closely related to how much the Earth warms in response to greenhouse gas increases. Here we find that the temperature response to an abrupt quadrupling of atmospheric carbon dioxide has increased substantially in the latest generation of global climate models. This is primarily because low cloud water content and coverage decrease more strongly with global warming, causing enhanced planetary absorption of sunlight—an amplifying feedback that ultimately results in more warming. Differences in the physical representation of clouds in models drive this enhanced sensitivity relative to the previous generation of models. It is crucial to establish whether the latest models, which presumably represent the climate system better than their predecessors, are also providing a more realistic picture of future climate warming.

Key Points:
- Climate sensitivity is larger on average in CMIP6 than in CMIP5 due mostly to a stronger positive low cloud feedback
- This is due to greater reductions in low cloud cover and weaker increases in low cloud water content, primarily in the extratropics
- These changes are related to model physics differences that are apparent in unforced climate variability

Supporting Information:
- Supporting Information S1

Correspondence to:
M. D. Zelinka,
zelinka1@llnl.gov

Citation:
Zelinka, M. D., Myers, T. A., McCoy, D. T., Po-Chedley, S., Caldwell, P. M., Ceppi, P., et al. (2020). Causes of higher climate sensitivity in CMIP6 models. *Geophysical Research Letters*, *47*, e2019GL085782. https://doi.org/10.1029/2019GL085782

Received 10 OCT 2019
Accepted 20 DEC 2019
Accepted article online 3 JAN 2020

1. Introduction

Determining the sensitivity of Earth's climate to changes in atmospheric carbon dioxide (CO_2) is a fundamental goal of climate science. A typical approach for doing so is to consider the planetary energy balance at the top of the atmosphere (TOA), represented as

$$R = F + \lambda T, \tag{1}$$

where R is the net TOA radiative flux anomaly, F is the radiative forcing, λ is the radiative feedback parameter, and T is the global mean surface air temperature anomaly. The sign convention is that R is positive down and λ is negative for a stable system. Conceptually, this equation states that the TOA energy imbalance can be expressed as the sum of the radiative forcing and the radiative response of the system to a global surface temperature anomaly. The assumption that the radiative damping can be expressed as a product of a time-invariant λ and global mean surface temperature anomaly is useful but imperfect (Armour et al., 2013; Ceppi & Gregory, 2019). Under this assumption, one can estimate the effective climate sensitivity (ECS), the ultimate global surface temperature change that would restore TOA energy balance ($R = 0$) in response to an instantaneous doubling of CO_2, as

$$\mathrm{ECS} = -F_{2\times}/\lambda, \tag{2}$$

where $F_{2\times}$ is the radiative forcing due to doubled CO_2.

ECS therefore depends on the magnitude of the CO_2 radiative forcing and on how strongly the climate system radiatively damps planetary warming. A climate system that more effectively radiates thermal energy

to space or more strongly reflects sunlight back to space as it warms (larger magnitude λ) will require less warming to restore planetary energy balance in response to a positive radiative forcing, and vice versa.

Hence despite being a simple scalar quantity, ECS encapsulates substantial information about the climate system and how it responds to perturbations. Moreover, despite being defined based on a hypothetical scenario, it has been shown to be a highly relevant measure of future climate impacts under more realistic scenarios (Grose et al., 2018) and for determining CO_2 stabilization targets to avoid crossing dangerous global temperature thresholds (Collins et al., 2013; Rogelj et al., 2014). A wide range of ECS values produced by global climate models (GCMs) or inferred using other approaches has persisted for decades (Knutti et al., 2017), though attempts to narrow this uncertainty by combining multiple lines of evidence appear promising (Stevens et al., 2016).

Because GCMs attempt to represent all relevant processes governing Earth's response to CO_2, they provide the most direct means of estimating ECS. ECS values diagnosed from CO_2 quadrupling experiments performed in fully coupled GCMs as part of the fifth phase of the Coupled Model Intercomparison Project (CMIP5; Taylor et al., 2012) ranged from 2.1 to 4.7 K (Andrews et al., 2012; Flato et al., 2014). It is already known that several models taking part in CMIP6 (Eyring et al., 2016) have values of ECS exceeding the upper limit of this range. These include CanESM5.0.3 (Swart et al., 2019), CESM2 (Gettelman et al., 2019), CNRM-CM6-1 (Voldoire et al., 2019), E3SMv1 (Golaz et al., 2019), and both HadGEM3-GC3.1 and UKESM1 (Andrews et al., 2019). In all of these models, high ECS values are at least partly attributed to larger cloud feedbacks than their predecessors.

In this study, we diagnose the forcings, feedbacks, and ECS values in all available CMIP6 models. We assess in each model the individual components that make up the climate feedback parameter and quantify the contributors to intermodel differences in ECS. We also compare these results with those from CMIP5 to determine whether the multimodel mean or spread in ECS, feedbacks, and forcings have changed.

2. Data and Methodology

We use output from fully coupled GCM experiments in which atmospheric CO_2 concentrations are abruptly quadrupled from their preindustrial concentrations and held fixed (abrupt-4xCO2). Anomalies are computed with respect to the corresponding time period in the preindustrial control simulations (piControl). Following Caldwell et al. (2016), we compute anomalies relative to a 21-year running average from piControl. This is done in an attempt to compute anomalies due to CO_2 while avoiding anomalies due solely to model drift, which we assume is equally present in both simulations but may not necessarily be monotonic.

Following Gregory et al. (2004), we regress global- and annual-mean TOA net downwelling radiative flux anomalies (R) on global- and annual-mean surface air temperature anomalies (T) to estimate effective radiative forcing (ERF_{2x}, y-intercept divided by 2), radiative feedback (λ, regression slope), and effective climate sensitivity (ECS, x-intercept divided by 2). The division by 2 is done so as to express ERF and ECS with respect to a CO_2 doubling, as is standard practice. The radiative forcing derived as such represents the net TOA imbalance due to the step change in CO_2 and rapid responses of the stratosphere and troposphere to the forcing, hence the qualifier "effective" (Sherwood et al., 2015). In many simulations, λ weakens as global temperature increases owing to evolving surface warming patterns (Andrews et al., 2015; Armour et al., 2013; Ceppi & Gregory, 2017) and to state-dependence in feedbacks (Bloch-Johnson et al., 2015; Meraner et al., 2013). Hence, the climate sensitivity derived using these 150-year simulations generally underestimates the warming that would be achieved at equilibrium (Rugenstein et al., 2019), which is why here and subsequently we refer to ECS as effective rather than equilibrium climate sensitivity (Gregory et al., 2004; Murphy, 1995). Scatterplots of R against T for all available CMIP6 models are shown in supporting information Figure S1, indicating the utility of equation (1) in diagnosing forcing, feedback, and ECS from abrupt-4xCO2 simulations.

To break down the feedback into individual components, we employ radiative kernels that quantify the sensitivity of TOA radiation to small perturbations in surface and atmospheric temperature, water vapor, and surface albedo (Soden et al., 2008; Shell et al., 2008). For each month of the 150-year experiment, spatially-resolved kernels are multiplied by the relevant climate field anomalies. These are then vertically integrated (in the case of feedbacks due to atmospheric temperature and water vapor) up to a time-varying

tropopause (Reichler et al., 2003) and then annually averaged to produce a 150-year time series of TOA radiative flux anomalies due to each field. These are then regressed on T to yield the individual radiative feedback components.

The cloud feedback is computed by adjusting the cloud radiative effect (CRE; clear- minus all-sky upwelling TOA flux) feedback for noncloud influences (Soden et al., 2008; Shell et al., 2008). In addition to the traditional temperature and water vapor feedbacks, we also consider an alternative formulation that decomposes these radiative feedbacks into a component due to warming and moistening at constant relative humidity and a component due to relative humidity changes (Held & Shell, 2012). Assumptions and approximations in the kernel technique require that we keep a residual feedback term. We use the Huang et al. (2017) kernels because they yield the smallest residuals, but all results are qualitatively unchanged when using Soden et al. (2008), Shell et al. (2008), Block and Mauritsen (2013), Pendergrass et al. (2018), or Smith et al. (2018) kernels (Figure S2 and Text S1).

To gain additional insights into the cloud feedback, we implement the approximate partial radiative perturbation (APRP) technique (Taylor et al., 2007), which yields estimates of the shortwave (SW) cloud feedback and its amount, scattering, and absorption components. The scattering component dominates the absorption component, so we combine these and refer to their sum as the "scattering" component, which is comparable to an optical depth feedback. Further details are provided in Text S2. Following Soden and Vecchi (2011), we separate cloud feedbacks into those due to low and non-low clouds using the Webb et al. (2006) method, which infers the cloud change responsible for the feedback by comparing the relative strengths of local longwave (LW) and SW cloud feedback components. Further details are provided in Text S3.

Throughout, we determine the statistical significance of CMIP5-to-CMIP6 differences using Welch's t-test for equal means and Bartlett's test for equal variances. Several modeling centers provided results from two or more closely related models. To avoid overstating statistical significance (Caldwell et al., 2014), we average results from all models from single modeling centers as a last step before performing all significance tests. This reduces the CMIP5 and CMIP6 sample sizes from 28 to 17 and from 27 to 19, respectively. Despite the fact that models from different centers may also be related (Knutti et al., 2013; Sanderson et al., 2015), we use this approach because accurately defining model independence is still an area of ongoing research and the required machinery would distract from the focus of this work. While we determine statistical significance using a 95% confidence level, we caution that changes can still be large and worthy of attention despite not reaching this threshold. Therefore, for several key results, we also report p values.

3. Results

3.1. Global Mean Quantities

In Figures 1a to 1c, we show estimates of ECS, ERF_{2x}, and global mean radiative feedbacks from all CMIP5 and CMIP6 models that provided the necessary diagnostics as of 27 November 2019. The traditional feedback breakdown, in which Planck and LR feedbacks are computed holding specific humidity fixed and the water vapor feedback is due solely to specific humidity changes, is shown in Figure S3. Feedback, forcing, and ECS values for each model are provided in Tables S1 and S2.

The range of ECS values across models has widened in CMIP6, particularly on the high end, and now includes nine models with values exceeding the CMIP5 maximum (Figure 1a). Specifically, the range has increased from 2.1–4.7 K in CMIP5 to 1.8–5.6 K in CMIP6, and the intermodel variance has significantly increased ($p = 0.04$). One model's ECS is below the CMIP5 minimum (INM-CM4-8). This increased population of high ECS models has caused the multimodel mean ECS to increase from 3.3 K in CMIP5 to 3.9 K in CMIP6. Though substantial, this increase is not statistically significant ($p = 0.16$). ERF_{2x} has increased slightly on average in CMIP6 and its intermodel standard deviation has been reduced by nearly 30% from 0.50 Wm^{-2} in CMIP5 to 0.36 Wm^{-2} in CMIP6 (Figure 1b).

With the exception of a slight decrease in the variance of the surface albedo feedback, the mean and variance in noncloud feedbacks are essentially unchanged between collections (Figure 1c). In contrast, average net cloud feedback is more positive in CMIP6. This increase is due primarily to the SW component, which has a noticeably bimodal distribution, and is slightly opposed by the LW component. Hence the apparent but statistically insignificant increase in mean λ (i.e., toward weaker radiative damping) is solely due to the strengthened positive cloud feedback. As with previous generations of models (Cess et al., 1989; Cess, 1990;

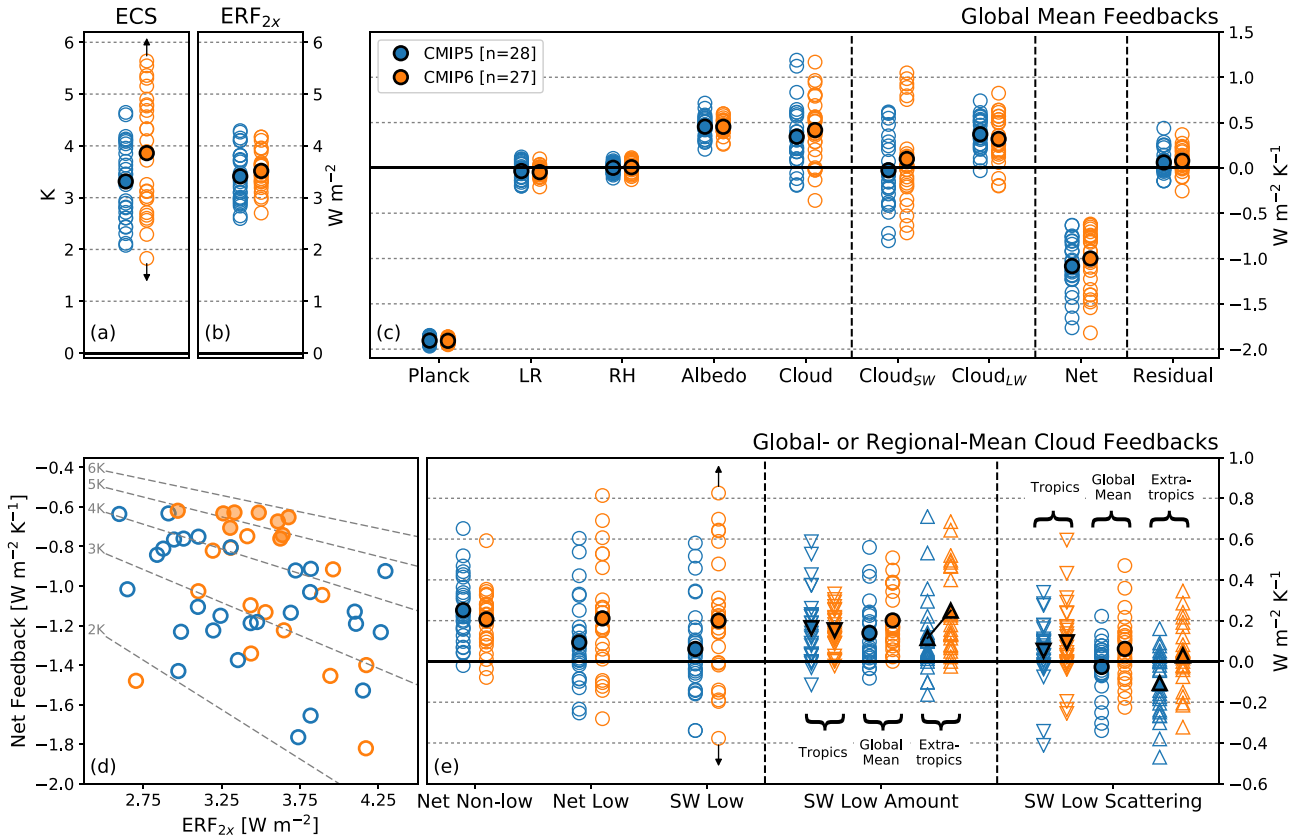

Figure 1. Estimates of (a) ECS, (b) ERF_{2x}, and (c) radiative feedbacks from abrupt-4xCO2 experiments. Individual CMIP5 and CMIP6 models are shown with unfilled blue and orange circles, respectively, and their multimodel averages are shown with filled circles. The total radiative feedback is broken down into Planck, lapse rate, relative humidity, surface albedo, and net cloud components. The cloud feedback is further broken down into its SW and LW components. Net refers to the net radiative feedback computed directly from TOA fluxes. The residual is the difference between the directly calculated net feedback and that estimated by summing kernel-derived components. (d) Net radiative feedback parameter plotted against ERF_{2x}. Dashed lines indicate constant ECS isopleths calculated using equation (2). Filled markers indicate models with ECS exceeding the maximum value in CMIP5. (e) Breakdown of the cloud feedback into net non-low, net low, and SW low components. The SW low component is further broken down into amount and scattering components, with tropical and extratropical means shown in triangles and global means shown in circles. Multimodel means that are significantly different ($p < 0.05$) are connected with a solid line. Intermodel variances that are significantly smaller or larger in CMIP6 ($p < 0.05$) are indicated with arrows pointing toward or away from the CMIP6 mean, respectively.

Dufresne & Bony, 2008; Soden & Held, 2006; Webb et al., 2013), the cloud feedback exhibits the largest intermodel spread of all feedbacks and is highly correlated with ECS in both collections (Figure S4A). Residuals in the kernel decomposition can be substantial in some models, but on average, they are near-zero in both collections. Kernel- and APRP-computed SW cloud feedbacks agree closely (Figure S5), indicating that the kernel decomposition is accurate.

Whereas both ERF_{2x} and λ have increased on average in CMIP6, their distributions do not extend beyond the CMIP5 range. Given these relatively subtle changes, how do nine CMIP6 models achieve higher ECS than seen in CMIP5? This result arises because these models have an unprecedented *combination* of forcing and feedback (Figure 1d; filled markers), as also noted by Andrews et al. (2019) for the HadGEM3-GC3.1 and UKESM1 models: CMIP6 models with the smallest magnitude λ (i.e., those having the strongest positive feedbacks offsetting Planck cooling) exhibit near-average ERF_{2x}. In contrast, the CMIP5 models with smallest magnitude λ had the weakest forcing. This feature is apparent from Figure 1d, where the $ERF_{2x} - \lambda$ space occupied by the models crosses more ECS isopleths in CMIP6 than in CMIP5.

Given that ERF_{2x} and λ have both increased on average in CMIP6, it is important to determine their relative importance in causing mean ECS to increase. We compute the hypothetical ECS distribution that would exist if the CMIP5 mean ERF_{2x} were increased to equal that in CMIP6 but the CMIP5 mean λ and ERF_{2x}-λ anticorrelation remained fixed. To do so, we shift each CMIP5 model's ERF_{2x} by the mean ERF_{2x} difference

between CMIP6 and CMIP5. We do the same transformation of the CMIP6 distribution (in reverse) and average the two results (Figure S6). Shifting $ERF_{2\times}$ changes ECS by 0.11 K on average, which is only 20% of the actual CMIP5-to-CMIP6 mean ECS difference of 0.55 K. In contrast, when we instead uniformly shift each model's λ so that the multimodel mean λ equals that in the other collection while keeping all else fixed, the mean ECS changes by 0.33 K, which is 61% of the actual difference. Shifting both $ERF_{2\times}$ and λ together changes mean ECS by 0.44 K, 81% of the difference. The remainder is accounted for by changes in the strength of the covariance between $ERF_{2\times}$ and λ.

From this, we conclude that while the highest ECS values in CMIP6 result from a combination of moderate forcing and weak negative feedback that did not occur in CMIP5, increased mean feedback alone (which arises from a stronger positive cloud feedback) is capable of increasing the multimodel mean ECS by most of the observed amount. Its contribution to increased ECS is three times larger than that of increased forcing. Consequently, we now turn to understanding what drives the increase in CMIP6 cloud feedback strength.

3.2. Detailing the Cloud Feedbacks

Whereas the net non-low cloud feedback is positive in all but two models with a mean that is slightly reduced from CMIP5, the distribution of net low cloud feedback is shifted toward larger positive values (with the mean increasing from 0.09 to 0.21 Wm^{-2} K^{-1}; Figure 1e). As expected, the increase in mean low cloud feedback is almost entirely due to the SW component, which exhibits significantly larger intermodel variance than in CMIP5 ($p = 0.046$) and is highly correlated with ECS in both collections (Figure S4B). Both amount and scattering components contribute to the increase in multimodel mean SW low cloud feedback (Figure 1e). Notably, the positive feedback from decreasing low cloud coverage has strengthened in CMIP6, and there are no longer any models with negative low cloud amount feedbacks. Additionally, the previously small negative feedback from changes in low cloud scattering is now positive on average in CMIP6.

To better understand how these feedbacks have changed, Figure 2a shows the zonally averaged SW low cloud feedback for the CMIP5 and CMIP6 multimodel means and their difference. Whereas the zonal mean SW low cloud feedback in CMIP5 exhibited a nearly symmetric latitudinal dipole centered at about 50° S, this feature is much less symmetric in CMIP6, with large positive values between 30–50° S and only a small region of weak negative values poleward of 60° S. The weak negative SW low cloud feedback poleward of about 50° N in CMIP5 is now weak and positive in CMIP6. Hence throughout the extratropics, the multimodel mean feedback is substantially more positive in CMIP6 (Figure 2a black line). These changes are similar to those seen in CESM1-CAM5 experiments in which the treatment of mean-state supercooled liquid fraction is modified to better match observations (Frey & Kay, 2017; Tan et al., 2016), and in the evolution of HadGEM3-GC2 to HadGEM3-GC3.1 (Bodas-Salcedo et al., 2019) and CESM1 to CESM2 (Gettelman et al., 2019).

Both the amount and scattering components are responsible for these extratropical increases. The multimodel mean SW low cloud amount component has increased by about 50% near its peak at 40° S and exhibits a much weaker and nonrobust negative feedback poleward of about 60° S (Figure 2b). This feedback is positive everywhere except poleward of 60° S and 75° N in the CMIP6 multimodel mean. Whereas CMIP5 models exhibited strong and robust negative extratropical scattering feedbacks, in CMIP6, these have been dramatically reduced (Figure 2c). Moreover, the CMIP6 mean SW low cloud scattering feedback is robustly positive between 30° and 45° S, with a large peak at about 40° S.

In sum, extratropical (poleward of 30°) mean SW low cloud amount feedback has increased markedly and significantly in CMIP6 ($p = 0.01$; Figure 1e). The extratropical mean SW low cloud scattering feedback has increased by roughly the same amount, but the change is not statistically significant ($p = 0.11$). In contrast, the change in tropical (equatorward of 30°) components is much smaller. Notably, the mean extratropical SW low cloud scattering feedback changes sign from negative in CMIP5 to positive in CMIP6, and the CMIP6 mean low cloud amount feedback is actually larger in the extratropics than in the tropics, which is remarkable given the latitudinal gradient of insolation (Figure 1e). Following Dufresne and Bony (2008) and Vial et al. (2013) as detailed in Text S4, we estimate that on average across CMIP6 models, the extratropical cloud feedback contributes 0.4 K of the 1.0 K cloud feedback-induced global temperature change (Figure S7). This proportion is roughly three times larger than in CMIP5 (0.1 K of 0.7 K). It is also clear from Figure S7, which shows the global temperature change induced by the forcing and each feedback in individual models, that large positive extratropical cloud feedbacks play a crucial role in allowing several CMIP6 models to achieve very high ECS. While the cloud feedback is on average the dominant cause of increased

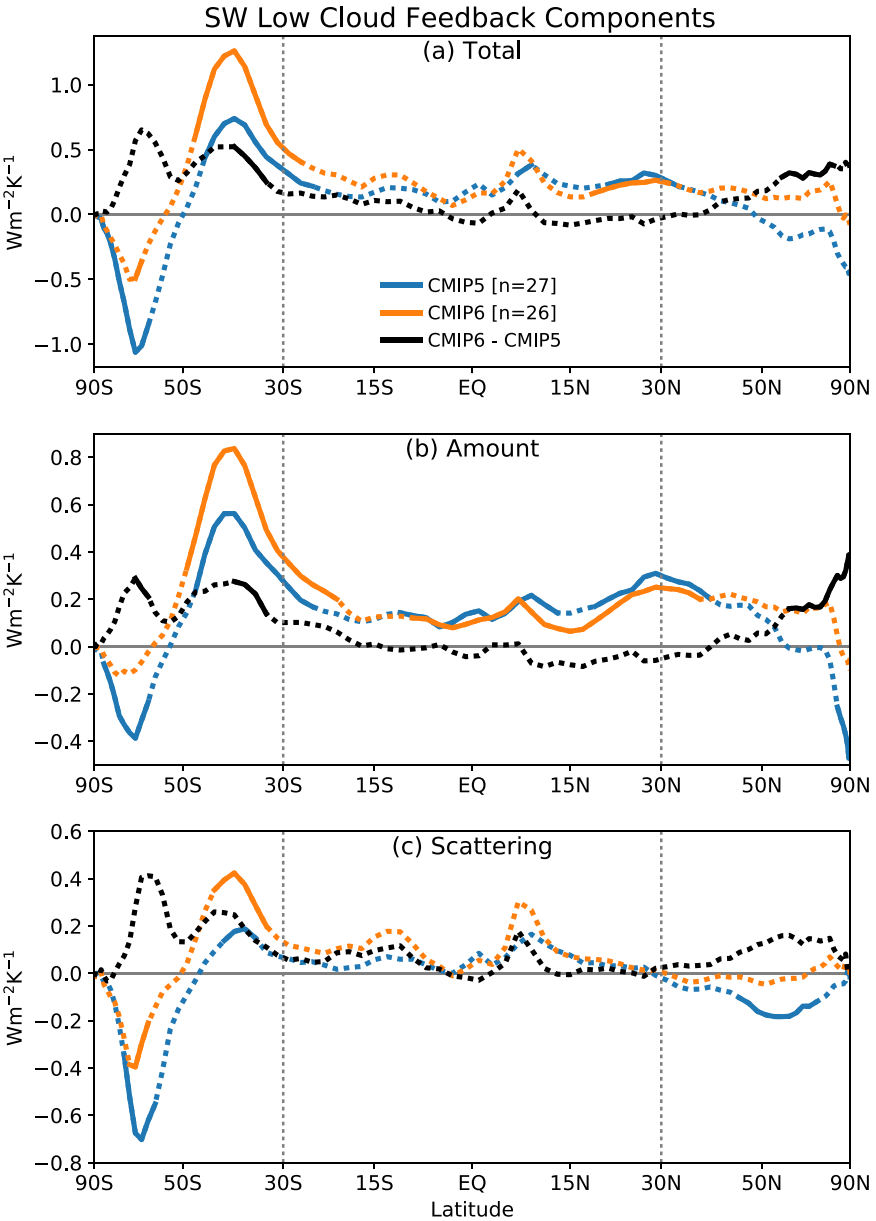

Figure 2. (a) Zonal mean SW low cloud feedback and its breakdown into (b) amount and (c) scattering components for the (blue) CMIP5 and (orange) CMIP6 multimodel means. Latitudes where at least 80% of the models agree on the sign of the feedback are plotted with a solid line. Multimodel mean differences are shown in black lines, which are solid where differences are significant ($p < 0.05$). Results are plotted against the sine of latitude to display uniform area weighting.

ECS in CMIP6, changes in other feedbacks and forcing can play non-negligible roles in driving higher ECS in individual models (Figure S7). Similarly, our explanation for the increase in CMIP6 mean cloud feedback need not apply to each individual model (Figure S8).

Finally, we find that the tropical SW low cloud amount feedback is positive in all but one CMIP6 model and its intermodel spread has decreased ($p = 0.08$). This may indicate the long-standing uncertainty in this feedback (Bony & Dufresne, 2005) is decreasing as tighter observational and high resolution modeling targets are established (Bretherton, 2015; Klein et al., 2017).

3.3. Physical Mechanisms for Larger Cloud Feedbacks in CMIP6

Why have the extratropical low cloud amount and scattering feedbacks increased in CMIP6? Across models, changes in low cloud amount, optical depth, and radiative effects with global warming have been shown

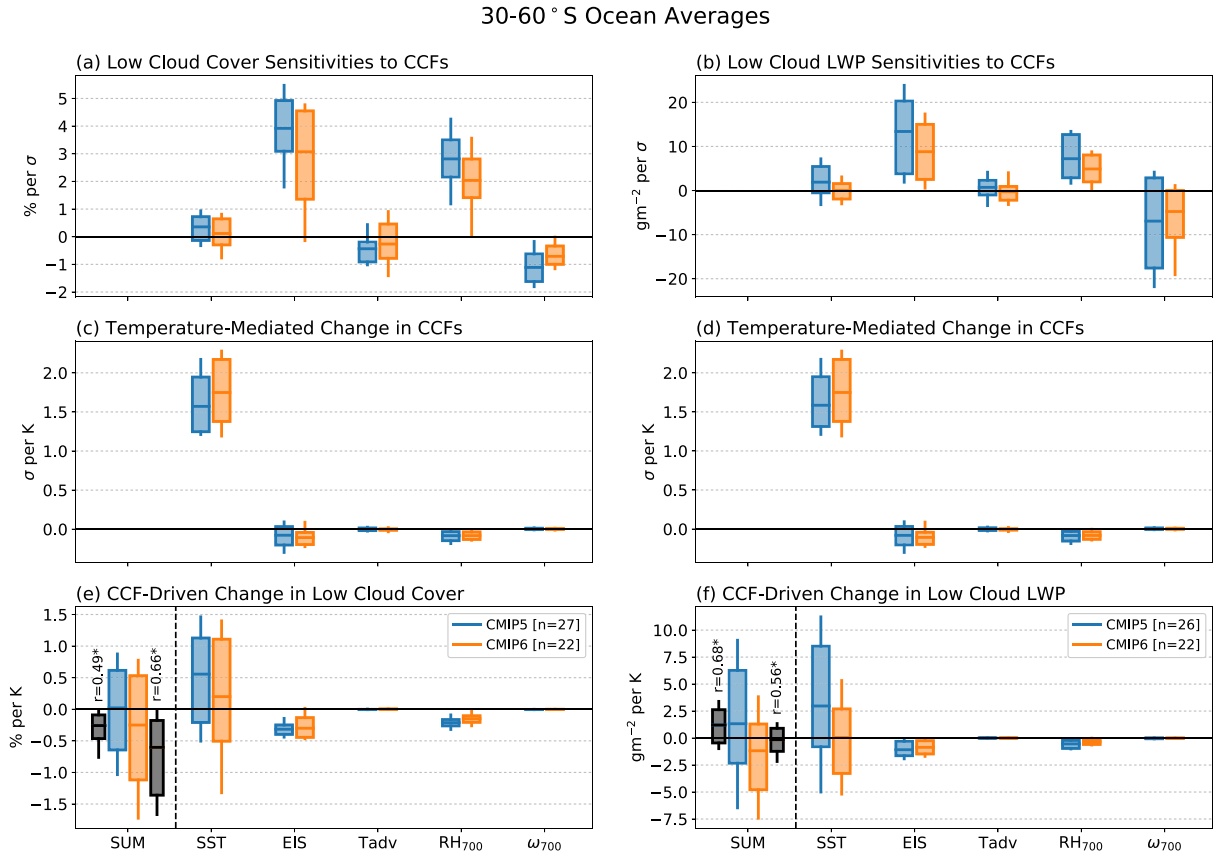

Figure 3. Sensitivities of (a) LCC and (b) LWP_{low} to sea surface temperature (*SST*), estimated inversion strength (*EIS*), surface temperature advection (*Tadv*), relative humidity at 700 hPa (RH_{700}), and pressure vertical velocity at 700 hPa (ω_{700}) estimated from climate variability over the SH midlatitude oceans (30° –60° S) in the piControl simulation. The changes in these factors per unit global warming from the abrupt-4xCO2 simulation are shown in (c) and (d). Predicted changes in (e) LCC and (f) LWP_{low} due to each cloud controlling factor, estimated as the product of the sensitivities shown in (a) and (b) with the multimodel mean responses of the quantities shown in (c) and (d). Black boxplots show the actual model-produced changes in LCC and LWP_{low} for (left) CMIP5 and (right) CMIP6, above which the across-model correlations between actual and predicted changes are printed. Asterisks indicate statistically significant correlation coefficients ($p < 0.05$). Boxes extend from the 17th to 83rd percentiles of the model values, with a line at the multimodel average. Whiskers extend to the 5th and 95th percentiles. Anomalies in cloud controlling factors are normalized by the standard deviation of their interannual variations in ERA5 (Copernicus Climate Change Service, 2017) and are therefore expressed in σ units, which aids intercomparison of quantities having different units.

to be well-predicted by the product of two terms: the sensitivity of cloud properties to cloud controlling factors (CCFs; Stevens & Brenguier, 2009) and the change in the CCFs with warming (Brient & Schneider, 2016, Klein et al., 2017; Myers & Norris, 2016; McCoy et al., 2017; Qu et al., 2014, 2015). SST and estimated inversion strength (EIS; Wood & Bretherton, 2006) are commonly found to be the most important CCFs for driving future cloud changes. The sensitivities of cloud properties to CCFs are typically estimated via multilinear regression applied to interannual covariations of meteorology and clouds in the unperturbed climate. Models exhibit widely varying cloud sensitivities owing to diversity in how clouds, convection, and turbulence are represented via parameterized physics (Geoffroy et al., 2017; Qu et al., 2014). In contrast, changes in CCFs in response to global warming are in relatively better agreement among models as they are less dependent on unresolved processes (Klein et al., 2017; Myers & Norris, 2016; Qu et al., 2014). Hence intermodel differences in how cloud properties change with global warming are largely driven by widely varying sensitivities of clouds to CCFs.

Several recent studies have demonstrated the utility of cloud controlling factor analyses for understanding changes in extratropical low-level cloud properties. These include Gordon and Klein (2014) and Terai et al. (2016) for cloud optical depth, Ceppi et al. (2016) for liquid water path (LWP), Grise and Medeiros (2016) and Kelleher and Grise (2019) for SWCRE, and Zelinka et al. (2018) and Miyamoto et al. (2018) for low cloud cover (LCC). Encouraged by these studies, we apply CCF analysis to estimate how LCC and in-cloud

LWP for low clouds (LWP_{low}) depend on five CCFs in the piControl simulations. LCC and LWP_{low} anomalies are defined as total cloud cover and LWP anomalies, respectively, where local radiation anomalies are attributable to low clouds, following Webb et al. (2006). These cloud properties are chosen because their changes are strongly anticorrelated across models with low cloud amount and scattering feedbacks (Figure S9). We perform the analysis within the 30–60° S latitude band where the low cloud feedback exhibits largest changes from CMIP5 to CMIP6. Further details are provided in Text S5.

The multilinear regression model, while imperfect, predicts LCC and LWP_{low} feedbacks that are significantly correlated across models with actual model-produced values (see correlations printed in Figures 3e and 3f). It also correctly predicts both that LCC decreases are larger on average in CMIP6 and that the average LWP_{low} response changes sign from positive in CMIP5 to negative in CMIP6. These changes are primarily due to the SST-driven component: The positive dependence of both LCC and LWP_{low} on SST has weakened in CMIP6 (Figures 3a and 3b). This weakened SST sensitivity overwhelms the slightly larger increase in 30–60° S SST in CMIP6 (Figures 3c and 3d), causing the SST-driven increases in LCC and LWP_{low} to be markedly weaker in CMIP6 (Figures 3e and 3f). Hence increased extratropical cloud feedback can be traced primarily to the fact that, on average, low cloud cover and water content increase with SST in CMIP5 but exhibit little sensitivity to SST in CMIP6.

4. Conclusions and Discussion

In this study, we investigated forcing, feedbacks, and climate sensitivity in abrupt CO_2 quadrupling experiments conducted in the latest generation of fully coupled GCMs as part of CMIP6, with an eye toward determining similarities with and differences from the previous generation of models. Both the multimodel mean and intermodel variance in ECS have increased substantially in CMIP6 relative to CMIP5, though only the latter change is statistically significant at 95% confidence. This ECS increase is primarily attributable to an increased multimodel mean feedback parameter due to strengthened positive cloud feedbacks, as all noncloud feedbacks are essentially unchanged on average in CMIP6. However, it is the unique combination of weak overall negative feedback and moderate radiative forcing that allows several CMIP6 models to achieve high ECS values beyond the CMIP5 range.

The increase in cloud feedback arises solely from the strengthened SW low cloud component, while the non-low cloud feedback has slightly decreased. The SW low cloud feedback is larger on average in CMIP6 due to larger reductions in low cloud cover and weaker increases in cloud liquid water path with warming. Both of these changes are much more dramatic in the extratropics, such that the CMIP6 mean low cloud amount feedback is now stronger in the extratropics than in the tropics, and the fraction of multimodel mean ECS attributable to extratropical cloud feedback has roughly tripled.

The aforementioned increase in CMIP6 mean cloud feedback is related to changes in model representation of clouds. Specifically, both low cloud cover and water content increase less dramatically with SST in the middle latitudes as estimated from unforced climate variability in CMIP6. A plausible reason for these responses is an increase in mean-state supercooled liquid water in mixed-phase clouds—manifest as an increased liquid condensate fraction (LCF)—in CMIP6 (Text S6 and Figure S10). Models with larger mean-state LCF have been shown to experience weaker LWP increases with warming (Bodas-Salcedo et al., 2019; Gettelman et al., 2019; McCoy et al., 2015; Tan et al., 2016), qualitatively consistent with CMIP6 versus CMIP5 differences. To the extent that condensate sinks related to ice processes weaken with warming (Ceppi et al., 2016), condensate lifetime increases, thereby increasing cloud cover or opposing cloud cover reductions caused by other processes. This effect should be weaker in models with larger mean-state LCF (i.e., CMIP6 models), potentially allowing them to experience larger cloud cover reductions with warming. Establishing more rigorously the reasons for these changes and evaluating them against observations is important future work.

Despite the fact that small deviations from a linear relationship between R and T can be seen to varying degrees among models in Figure S1, in this work, we have computed ECS assuming invariant λ. ECS diagnosed ignoring the first 20 years of abrupt-4xCO2 anomalies (Andrews et al., 2015) is 6% larger on average, roughly half as large as the CMIP5 inflation factor of 11% (Figure S11). Future work should elucidate this in greater detail.

Relatedly, $ERF_{2\times}$ estimated via equation (1) is subject to substantial uncertainties (Andrews et al., 2012; Chung & Soden, 2015). Future studies should better quantify $ERF_{2\times}$ using fixed SST experiments

(Forster et al., 2016; Pincus et al., 2016). These experiments will also allow for a clearer elucidation of the various components of the rapid tropospheric adjustments to CO_2 that drive intermodel spread in $ERF_{2\times}$. These could also confirm whether the strengthened anticorrelation between $ERF_{2\times}$ and λ and the substantial reduction in intermodel spread in $ERF_{2\times}$ found here are robust results and provide reasons for them.

As more output from CMIP6 models becomes available, more detailed analysis of the cloud feedback will be possible (Cesana et al., 2019; Gordon & Klein, 2014; Terai et al., 2016; Tsushima et al., 2016; Zelinka et al., 2012a, 2012b, 2013, 2016), permitting better understanding of why the low cloud feedback has strengthened. Output from additional models might also refine the statistical significance of several intriguing results reported here, which based on the limited sample of models fall just short of being statistically significant. Because the number of models analyzed in this study (27 CMIP6 models from 19 distinct modeling centers) is much less than the 102 models from 35 centers expected to perform abrupt-4xCO2 and piControl experiments, we caution that some conclusions may change as more data become available.

ECS is higher on average in CMIP6 due primarily to strengthened cloud feedbacks. Tropical low cloud feedbacks and global non-low cloud feedbacks are positive in nearly every model. Extratropical low cloud scattering feedbacks have shifted to more positive values, which may be related to increases in mean-state supercooled liquid water in mixed-phase clouds. All of these are consistent with GCMs achieving a better qualitative match with theoretical, observational, and/or high-resolution modeling evidence for positive high cloud altitude feedback (Hartmann & Larson, 2002; Kuang & Hartmann, 2007; Thompson et al., 2017; Zelinka & Hartmann, 2011), positive tropical low cloud feedback (Bretherton, 2015; Klein et al., 2017), and weak negative or even positive extratropical low cloud scattering feedback (McCoy et al., 2015; Tan et al., 2016; Terai et al., 2016). This raises the possibility that ECS is indeed high in the real world, but it first needs to be established that CMIP6 feedbacks and forcing are in *quantitative* agreement with these constraints. It is possible, for example, that higher ECS in models from larger extratropical low cloud feedbacks might simply be revealing (as yet unknown) errors in other feedbacks. Such a conclusion would also need to be evaluated in light of other evidence. For example, how well do high ECS models simulate past climates or the historical record? While some high ECS models closely match the observed record (e.g., Gettelman et al., 2019), others do not (e.g., Golaz et al., 2019). Do the former models achieve their results via unreasonably large negative aerosol forcings and/or substantial pattern effects (Kiehl, 2007; Stevens et al., 2016)? It is worth noting that cloud feedbacks are enhanced in CMIP6 primarily over the Southern Ocean, a region of efficient ocean heat uptake (Armour et al., 2016). This implies that the enhanced surface SW heating is less likely to manifest as surface warming during transient climate change than if the heating were focused elsewhere (Frey et al., 2017). This cloud feedback pattern could make it easier for high ECS models to simulate the observed surface temperature record without requiring a large negative aerosol radiative forcing or large historical era pattern effects.

Acknowledgments
This work was performed under the auspices of the U.S. Department of Energy (DOE) by Lawrence Livermore National Laboratory under Contract DE-AC52-07NA27344. M.D.Z., T.A.M., P.M.C., S.A.K., and K.E.T. were supported by the Regional and Global Model Analysis Program of the Office of Science at the DOE. D.T.M. was supported by the PRIMAVERA project, funded by the European Union's Horizon 2020 programme, Grant Agreement no. 641727. S.P.-C. was supported by LLNL LDRD 18-ERD-054. P.C. was supported by an Imperial College Research Fellowship. We acknowledge the World Climate Research Programme, which, through its Working Group on Coupled Modelling, coordinated and promoted CMIP5 and CMIP6. We thank the climate modeling groups for producing and making available their model output, the Earth System Grid Federation (ESGF) for archiving the data and providing access, and the multiple funding agencies who support CMIP and ESGF. All CMIP data are available from the ESGF at https://esgf-node.llnl.gov/projects/esgf-llnl/. Finally, we thank Tim Andrews, Andrew Gettelman, Masahiro Watanabe, and an anonymous reviewer for critical comments that helped improve the manuscript.

References

Andrews, T., Andrews, M. B., Bodas-Salcedo, A., Jones, G. S., Kulhbrodt, T., Manners, J., & Tang, Y. (2019). Forcings, feedbacks and climate sensitivity in HadGEM3-GC3.1 and UKESM1. *Journal of Advances in Modeling Earth Systems*, *11*. https://doi.org/10.1029/2019MS001866

Andrews, T., Gregory, J. M., & Webb, M. J. (2015). The dependence of radiative forcing and feedback on evolving patterns of surface temperature change in climate models. *Journal of Climate*, *28*(4), 1630–1648. https://doi.org/10.1175/jcli-d-14-00545.1

Andrews, T., Gregory, J. M., Webb, M. J., & Taylor, K. E. (2012). Forcing, feedbacks and climate sensitivity in CMIP5 coupled atmosphere-ocean climate models. *Geophysical Research Letters*, *39*, L09712. https://doi.org/10.1029/2012GL051607

Armour, K. C., Bitz, C. M., & Roe, G. H. (2013). Time-varying climate sensitivity from regional feedbacks. *Journal of Climate*, *26*(13), 4518–4534. https://doi.org/10.1175/jcli-d-12-00544.1

Armour, K. C., Marshall, J., Scott, J. R., Donohoe, A., & Newsom, E. R. (2016). Southern Ocean warming delayed by circumpolar upwelling and equatorward transport. *Nature Geoscience*, *9*(7), 549–554. https://doi.org/10.1038/ngeo2731

Bloch-Johnson, J., Pierrehumbert, R. T., & Abbot, D. S. (2015). Feedback temperature dependence determines the risk of high warming. *Geophysical Research Letters*, *42*, 4973–4980. https://doi.org/10.1002/2015gl064240

Block, K., & Mauritsen, T. (2013). Forcing and feedback in the MPI-ESM-LR coupled model under abruptly quadrupled CO2. *Journal of Advances in Modeling Earth Systems*, *5*, 676–691. https://doi.org/10.1002/jame.20041

Bodas-Salcedo, A., Mulcahy, J. P., Andrews, T., Williams, K. D., Ringer, M. A., Field, P. R., & Elsaesser, G. S. (2019). Strong dependence of atmospheric feedbacks on mixed-phase microphysics and aerosol-cloud interactions in HadGEM3. *Journal of Advances in Modeling Earth Systems*, *11*, 1735–1758. https://doi.org/10.1029/2019MS001688

Bony, S., & Dufresne, J. L. (2005). Marine boundary layer clouds at the heart of tropical cloud feedback uncertainties in climate models. *Geophysical Research Letters*, *32*, L20806. https://doi.org/10.1029/2005GL023851

Bretherton, C. S. (2015). Insights into low-latitude cloud feedbacks from high-resolution models. *Philosophical Transactions of the Royal Society a-Mathematical Physical and Engineering Sciences*, *373*, 2054. https://doi.org/10.1098/rsta.2014.0415

Brient, F., & Schneider, T. (2016). Constraints on climate sensitivity from space-based measurements of low-cloud reflection. *Journal of Climate*, *29*(16), 5821–5835. https://doi.org/10.1175/JCLI-D-15-0897.1

Caldwell, P. M., Bretherton, C. S., Zelinka, M. D., Klein, S. A., Santer, B. D., & Sanderson, B. M. (2014). Statistical significance of climate sensitivity predictors obtained by data mining. *Geophysical Research Letters*, *41*, 1803–1808. https://doi.org/10.1002/2014GL059205

Caldwell, P. M., Zelinka, M. D., Taylor, K. E., & Marvel, K. (2016). Quantifying the sources of intermodel spread in equilibrium climate sensitivity. *Journal of Climate*, *29*(2), 513–524. https://doi.org/10.1175/jcli-d-15-0352.1

Ceppi, P., & Gregory, J. M. (2017). Relationship of tropospheric stability to climate sensitivity and Earth's observed radiation budget. *Proceedings of the National Academy of Sciences of the United States of America*, *114*(50), 13126–13131. https://doi.org/10.1073/pnas.1714308114

Ceppi, P., & Gregory, J. M. (2019). A refined model for the Earth's global energy balance. *Climate Dynamics*, *53*, 4781–4797. https://doi.org/10.1007/s00382-019-04825-x

Ceppi, P., Hartmann, D. L., & Webb, M. J. (2016). Mechanisms of the negative shortwave cloud feedback in middle to high latitudes. *Journal of Climate*, *29*(1), 139–157. https://doi.org/10.1175/jcli-d-15-0327.1

Cesana, G., Del Genio, A. D., Ackerman, A. S., Kelley, M., Elsaesser, G., Fridlind, A. M., & Yao, M. S. (2019). Evaluating models' response of tropical low clouds to SST forcings using CALIPSO observations. *Atmospheric Chemistry and Physics*, *19*(5), 2813–2832. https://doi.org/10.5194/acp-19-2813-2019

Cess, R. D. (1990). Intercomparison and interpretation of cloud-climate feedback processes in nineteen atmospheric general circulation models. *Journal of Geophysical Research*, *95*, 16,601–16,615.

Cess, R. D., Potter, G. L., Blanchet, J. P., Boer, G. J., Ghan, S. J., Kiehl, J. T., & Yagai, I. (1989). Interpretation of cloud-climate feedback as produced by 14 atmospheric general circulation models. *Science*, *245*(4917), 513–516. https://doi.org/10.1126/science.245.4917.513

Chung, E. S., & Soden, B. J. (2015). An assessment of methods for computing radiative forcing in climate models. *Environmental Research Letters*, *10*(7), 74004. https://doi.org/10.1088/1748-9326/10/7/074004

Collins, M., Knutti, R., Arblaster, J., Dufresne, J. L., Fichefet, T., Friedlingstein, P., & Wehner, M. (2013). Long-term climate change: Projections, commitments and irreversibility. In T. F. Stocker, D. Qin, G.-K. Plattner, M. M. B. Tignor, S. K. Allen, J. Boschung, et al. (Eds.), *Climate change 2013: The physical science basis. Contribution of working group I to the fifth assessment report of the intergovernmental panel on climate change* (pp. 1029–1136). Cambridge, United Kingdom and New York, NY, USA: Cambridge University Press.

Copernicus Climate Change Service (C3S) (2017). ERA5: Fifth generation of ECMWF atmospheric reanalyses of the global climate. Copernicus Climate Change Service Climate Data Store (CDS), 8 July 2018. https://cds.climate.copernicus.eu/cdsapp#!/home

Dufresne, J. L., & Bony, S. (2008). An assessment of the primary sources of spread of global warming estimates from coupled atmosphere–ocean models. *Journal of Climate*, *21*, 5135–5144. https://doi.org/10.1175/2008JCLI2239.1

Eyring, V., Bony, S., Meehl, G. A., Senior, C. A., Stevens, B., Stouffer, R. J., & Taylor, K. E. (2016). Overview of the Coupled Model Intercomparison Project Phase 6 (CMIP6) experimental design and organization. *Geoscientific Model Development*, *9*(5), 1937–1958. https://doi.org/10.5194/gmd-9-1937-2016

Flato, G., Marotzke, J., Abiodun, B., Braconnot, P., Chou, S. C., Collins, W., & Zhang, J. L. (2014). Evaluation of climate models. In *Evaluation of climate models. Climate change 2013 - The physical science basis: Working group I contribution to the fifth assessment report of the intergovernmental panel on climate change* (pp. 741–866). Cambridge: Cambridge University Press.

Forster, P. M., Richardson, T., Maycock, A. C., Smith, C. J., Samset, B. H., Myhre, G., & Schulz, M. (2016). Recommendations for diagnosing effective radiative forcing from climate models for CMIP6. *Journal of Geophysical Research: Atmospheres*, *121*, 12,460–12,475. https://doi.org/10.1002/2016JD025320

Frey, W. R., & Kay, J. E. (2017). The influence of extratropical cloud phase and amount feedbacks on climate sensitivity. *Climate Dynamics*, *50*, 3097. https://doi.org/10.1007/s00382-017-3796-5

Frey, W. R., Maroon, E. A., Pendergrass, A. G., & Kay, J. E. (2017). Do Southern Ocean cloud feedbacks matter for 21st century warming? *Geophysical Research Letters*, *44*, 12,447–12,456. https://doi.org/10.1002/2017GL076339

Geoffroy, O., Sherwood, S. C., & Fuchs, D. (2017). On the role of the stratiform cloud scheme in the inter-model spread of cloud feedback. *Journal of Advances in Modeling Earth Systems*, *9*, 423–437. https://doi.org/10.1002/2016MS000846

Gettelman, A., Hannay, C., Bacmeister, J. T., Neale, R. B., Pendergrass, A. G., Danabasoglu, G., & Mills, M. J. (2019). High climate sensitivity in the community Earth system model version 2 (CESM2). *Geophysical Research Letters*, *46*, 8329–8337. https://doi.org/10.1029/2019GL083978

Golaz, J. C., Caldwell, P. M., Van Roekel, L. P., Petersen, M. R., Tang, Q., Wolfe, J. D., & Zhu, Q. (2019). The DOE E3SM coupled model version 1: Overview and evaluation at standard resolution. *Journal of Advances in Modeling Earth Systems*, *11*, 2089–2129. https://doi.org/10.1029/2018ms001603

Gordon, N. D., & Klein, S. A. (2014). Low-cloud optical depth feedback in climate models. *Journal of Geophysical Research: Atmospheres*, *119*, 6052–6065. https://doi.org/10.1002/2013JD021052

Gregory, J. M., Ingram, W. J., Palmer, M. A., Jones, G. S., Stott, P. A., Thorpe, R. B., & Williams, K. D. (2004). A new method for diagnosing radiative forcing and climate sensitivity. *Geophysical Research Letters*, *31*, L03205. https://doi.org/10.1029/2003GL018747

Grise, K. M., & Medeiros, B. (2016). Understanding the varied influence of midlatitude jet position on clouds and cloud radiative effects in observations and global climate models. *Journal of Climate*, *29*(24), 9005–9025. https://doi.org/10.1175/jcli-d-16-0295.1

Grose, M. R., Gregory, J., Colman, R., & Andrews, T. (2018). What climate sensitivity index is most useful for projections? *Geophysical Research Letters*, *45*, 1559–1566. https://doi.org/10.1002/2017GL075742

Hartmann, D. L., & Larson, K. (2002). An important constraint on tropical cloud-climate feedback. *Geophysical Research Letters*, *29*, 1951. https://doi.org/10.1029/2002GL015835

Held, I. M., & Shell, K. M. (2012). Using relative humidity as a state variable in climate feedback analysis. *Journal of Climate*, *25*(8), 2578–2582. https://doi.org/10.1175/JCLI-D-11-00721.1

Huang, Y., Xia, Y., & Tan, X. X. (2017). On the pattern of CO2 radiative forcing and poleward energy transport. *Journal of Geophysical Research: Atmospheres*, *122*, 10,578–10,593. https://doi.org/10.1002/2017JD027221

Kelleher, M. K., & Grise, K. M. (2019). Examining Southern Ocean cloud controlling factors on daily time scales and their connections to midlatitude weather systems. *Journal of Climate*, *32*(16), 5145–5160. https://doi.org/10.1175/jcli-d-18-0840.1

Kiehl, J. T. (2007). Twentieth century climate model response and climate sensitivity. *Geophysical Research Letters*, *34*, L22710. https://doi.org/10.1029/2007GL031383

Klein, S. A., Hall, A., Norris, J. R., & Pincus, R. (2017). Low-cloud feedbacks from cloud-controlling factors: A review. *Surveys in Geophysics*, *38*, 1307–1329. https://doi.org/10.1007/s10712-017-9433-3

Knutti, R., Masson, D., & Gettelman, A. (2013). Climate model genealogy: Generation CMIP5 and how we got there. *Geophysical Research Letters*, *40*, 1194–1199. https://doi.org/10.1002/grl.50256

Knutti, R., Rugenstein, M. A. A., & Hegerl, G. C. (2017). Beyond equilibrium climate sensitivity. *Nature Geoscience*, *10*, 727. https://doi.org/10.1038/ngeo3017

Kuang, Z., & Hartmann, D. L. (2007). Testing the fixed anvil temperature hypothesis in a cloud-resolving model. *Journal Climate*, *20*, 2051–2057. https://doi.org/10.1175/JCLI4124.1

McCoy, D. T., Eastman, R., Hartmann, D. L., & Wood, R. (2017). The change in low cloud cover in a warmed climate inferred from AIRS, MODIS and ECMWF-Interim reanalysis. *Journal of Climate*, *30*, 3609–3620. https://doi.org/10.1175/JCLI-D-15-0734.1

McCoy, D. T., Hartmann, D. L., Zelinka, M. D., Ceppi, P., & Grosvenor, D. P. (2015). Mixed-phase cloud physics and Southern Ocean cloud feedback in climate models. *Journal of Geophysical Research: Atmospheres*, *120*, 9539–9554. https://doi.org/10.1002/2015JD023603

Meraner, K., Mauritsen, T., & Voigt, A. (2013). Robust increase in equilibrium climate sensitivity under global warming. *Geophysical Research Letters*, *40*, 5944–5948. https://doi.org/10.1002/2013gl058118

Miyamoto, A., Nakamura, H., & Miyasaka, T. (2018). Influence of the subtropical high and storm track on low-cloud fraction and its seasonality over the South Indian Ocean. *Journal of Climate*, *31*(10), 4017–4039. https://doi.org/10.1175/jcli-d-17-0229.1

Murphy, J. M. (1995). TRAnsient-response of the hadley center coupled ocean-atmosphere model to increasing carbon-dioxide .3. analysis of global-mean response using simple-models. *Journal of Climate*, *8*(3), 496–514. https://doi.org/10.1175/1520-0442(1995)008<0496:trothc>2.0.CO;2

Myers, T. A., & Norris, J. R. (2016). Reducing the uncertainty in subtropical cloud feedback. *Geophysical Research Letters*, *43*, 2144–2148. https://doi.org/10.1002/2015GL067416

Pendergrass, A. G., Conley, A., & Vitt, F. M. (2018). Surface and top-of-atmosphere radiative feedback kernels for CESM-CAM5. *Earth System Science Data*, *10*(1), 317–324. https://doi.org/10.5194/essd-10-317-2018

Pincus, R., Forster, P. M., & Stevens, B. (2016). The radiative forcing model intercomparison project (RFMIP): Experimental protocol for CMIP6. *Geoscientific Model Development*, *9*(9), 3447–3460. https://doi.org/10.5194/gmd-9-3447-2016

Qu, X., Hall, A., Klein, S. A., & Caldwell, P. M. (2014). On the spread of changes in marine low cloud cover in climate model simulations of the 21st century. *Climate Dynamics*, *42*(9-10), 2603–2626. https://doi.org/10.1007/s00382-013-1945-z

Qu, X., Hall, A., Klein, S. A., & DeAngelis, A. M. (2015). Positive tropical marine low-cloud cover feedback inferred from cloud-controlling factors. *Geophysical Research Letters*, *42*, 7767–7775. https://doi.org/10.1002/2015GL065627

Reichler, T., Dameris, M., & Sausen, R. (2003). Determining the tropopause height from gridded data. *Geophysical Research Letters*, *30*(20), 2042. https://doi.org/10.1029/2003GL018240

Rogelj, J., Meinshausen, M., Sedlacek, J., & Knutti, R. (2014). Implications of potentially lower climate sensitivity on climate projections and policy. *Environmental Research Letters*, *9*(3), 031003. https://doi.org/10.1088/1748-9326/9/3/031003

Rugenstein, M., Bloch-Johnson, J., Gregory, J., Andrews, T., Mauritsen, T., Li, C., & Knutti, R. (2019). Equilibrium climate sensitivity estimated by equilibrating climate models. *Geophysical Research Letters*, *46*. https://doi.org/10.1029/2019GL083898

Sanderson, B. M., Knutti, R., & Caldwell, P. (2015). A representative democracy to reduce interdependency in a multimodel ensemble. *Journal of Climate*, *28*(13), 5171–5194. https://doi.org/10.1175/jcli-d-14-00362.1

Shell, K. M., Kiehl, J. T., & Shields, C. A. (2008). Using the radiative kernel technique to calculate climate feedbacks in NCAR's community atmospheric model. *Journal Climate*, *21*(10), 2269–2282. https://doi.org/10.1175/2007JCLI2044.1

Sherwood, S. C., Bony, S., Boucher, O., Bretherton, C., Forster, P. M., Gregory, J. M., & Stevens, B. (2015). Adjustments in the forcing-feedback framework for understanding climate change. *Bulletin of the American Meteorological Society*, *96*(2), 217–228. https://doi.org/10.1175/bams-d-13-00167.1

Smith, C. J., Kramer, R. J., Myhre, G., Forster, P. M., Soden, B. J., Andrews, T., & Watson-Parris, D. (2018). Understanding rapid adjustments to diverse forcing agents. *Geophysical Research Letters*, *45*, 12,023–12,031. https://doi.org/10.1029/2018GL079826

Soden, B. J., & Held, I. M. (2006). An assessment of climate feedbacks in coupled ocean-atmosphere models. *Journal Climate*, *19*, 3354–3360. https://doi.org/10.1175/JCLI3799.1

Soden, B. J., Held, I. M., Colman, R., Shell, K. M., Kiehl, J. T., & Shields, C. A. (2008). Quantifying climate feedbacks using radiative kernels. *Journal Climate*, *21*, 3504–3520. https://doi.org/10.1175/2007JCLI2110.1

Soden, B. J., & Vecchi, G. A. (2011). The vertical distribution of cloud feedback in coupled ocean-atmosphere models. *Geophysical Research Letters*, *38*, L12704. https://doi.org/10.1029/2011GL047632

Stevens, B., & Brenguier, J. L. (2009). Cloud-controlling factors low clouds, *Clouds in the perturbed climate system: Their relationship to energy balance, atmospheric dynamics, and precipitation* (pp. 173–196). Cambridge, Mass: MIT Press.

Stevens, B., Sherwood, S. C., Bony, S., & Webb, M. J. (2016). Prospects for narrowing bounds on Earth's equilibrium climate sensitivity. *Earths Future*, *4*, 512–522. https://doi.org/10.1002/2016EF000376

Swart, N. C., Cole, J. N. S., Kharin, V. V., Lazare, M., Scinocca, J. F., Gillett, N. P., & Winter, B. (2019). The Canadian Earth System Model version 5 (CanESM5.0.3). *Geoscientific Model Development Discuss*, *2019*, 1–68. https://doi.org/10.5194/gmd-2019-177

Tan, I., Storelvmo, T., & Zelinka, M. D. (2016). Observational constraints on mixed-phase clouds imply higher climate sensitivity. *Science*, *352*(6282), 224–227. https://doi.org/10.1126/science.aad5300

Taylor, K. E., Crucifix, M., Braconnot, P., Hewitt, C. D., Doutriaux, C., Broccoli, A. J., & Webb, M. J. (2007). Estimating shortwave radiative forcing and response in climate models. *Journal Climate*, *20*(11), 2530–2543. https://doi.org/10.1175/JCLI4143.1

Taylor, K. E., Stouffer, R. J., & Meehl, G. A. (2012). An overview of CMIP5 and the experiment design. *Bulletin of the American Meteorological Society*, *93*(4), 485–498. https://doi.org/10.1175/BAMS-D-11-00094.1

Terai, C. R., Klein, S. A., & Zelinka, M. D. (2016). Constraining the low-cloud optical depth feedback at middle and high latitudes using satellite observations. *Journal of Geophysical Research: Atmospheres*, *121*, 9696–9716. https://doi.org/10.1002/2016JD025233

Thompson, D. W. J., Bony, S., & Li, Y. (2017). Thermodynamic constraint on the depth of the global tropospheric circulation. *Proceedings of the National Academy of Sciences*, *114*, 8181–8186. https://doi.org/10.1073/pnas.1620493114

Tsushima, Y., Ringer, M. A., Koshiro, T., Kawai, H., Roehrig, R., Cole, J., & Webb, M. J. (2016). Robustness, uncertainties, and emergent constraints in the radiative responses of stratocumulus cloud regimes to future warming. *Climate Dynamics*, *46*(9), 3025–3039. https://doi.org/10.1007/s00382-015-2750-7

Vial, J., Dufresne, J. L., & Bony, S. (2013). On the interpretation of inter-model spread in CMIP5 climate sensitivity estimates. *Climate Dynamics*, *41*(11-12), 3339–3362. https://doi.org/10.1007/s00382-013-1725-9

Voldoire, A., Saint-Martin, D., Senesi, S., Decharme, B., Alias, A., Chevallier, M., & Waldman, R. (2019). Evaluation of CMIP6 DECK experiments with CNRM-CM6-1. *Journal of Advances in Modeling Earth Systems*, *11*, 2177–2213. https://doi.org/10.1029/2019MS001683

Webb, M. J., Lambert, F. H., & Gregory, J. M. (2013). Origins of differences in climate sensitivity, forcing and feedback in climate models. *Climate Dynamics*, *40*(3-4), 677–707. https://doi.org/10.1007/s00382-012-1336-x

Webb, M. J., Senior, C. A., Sexton, D. M. H., Ingram, W. J., Williams, K. D., Ringer, M. A., & Taylor, K. E. (2006). On the contribution of local feedback mechanisms to the range of climate sensitivity in two GCM ensembles. *Climate Dynamite*, *27*, 17–38. https://doi.org/10.1007/s00382-006-0111-2

Wood, R., & Bretherton, C. S. (2006). On the relationship between stratiform low cloud cover and lower-tropospheric stability. *Journal Climate*, *19*(24), 6425–6432. https://doi.org/10.1175/JCLI3988.1

Zelinka, M. D., Grise, K. M., Klein, S. A., Zhou, C., DeAngelis, A. M., & Christensen, M. W. (2018). Drivers of the low-cloud response to poleward jet shifts in the North Pacific in observations and models. *Journal of Climate*, *31*(19), 7925–7947. https://doi.org/10.1175/jcli-d-18-0114.1

Zelinka, M. D., & Hartmann, D. L. (2011). The observed sensitivity of high clouds to mean surface temperature anomalies in the tropics. *Journal of Geophysical Research*, *116*, D23103. https://doi.org/10.1029/2011JD016459

Zelinka, M. D., Klein, S. A., & Hartmann, D. L. (2012a). Computing and partitioning cloud feedbacks using cloud property histograms. Part I: Cloud radiative kernels. *Journal of Climate*, *25*(11), 3715–3735. https://doi.org/10.1175/jcli-d-11-00248.1

Zelinka, M. D., Klein, S. A., & Hartmann, D. L. (2012b). Computing and partitioning cloud feedbacks using cloud property histograms. Part II: Attribution to changes in cloud amount, altitude, and optical depth. *Journal of Climate*, *25*(11), 3736–3754. https://doi.org/10.1175/JCLI-D-11-00249.1

Zelinka, M. D., Klein, S. A., Taylor, K. E., Andrews, T., Webb, M. J., Gregory, J. M., & Forster, P. M. (2013). Contributions of different cloud types to feedbacks and rapid adjustments in CMIP5. *Journal of Climate*, *26*(14), 5007–5027. https://doi.org/10.1175/jcli-d-12-00555.1

Zelinka, M. D., Zhou, C., & Klein, S. A. (2016). Insights from a refined decomposition of cloud feedbacks. *Geophysical Research Letters*, *43*, 9259–9269. https://doi.org/10.1002/2016GL069917